

Supporting Information

Utilizing Native Lignin as Redox-Active Material in Conductive Wood for Electronic and Energy Storage Applications

Van Chinh Tran ^{1,2}, Gabriella G. Mastantuoni ^{3,4}, Dagmawi Belaineh ^{1,5}, Selda Aminzadeh ⁴,
Lars A. Berglund ⁴, Magnus Berggren* ^{1,2}, Qi Zhou ^{3,4}, Isak Engquist* ^{1,2}.

¹ *Laboratory of Organic Electronics, Department of Science and Technology, Linköping University, 60174 Norrköping, Sweden.*

² *Wallenberg Wood Science Center, ITN, Linköping University, SE-601 74 Norrköping, Sweden*

³ *Division of Glycoscience, Department of Chemistry, KTH Royal Institute of Technology, AlbaNova University Centre, 106 91 Stockholm, Sweden.*

⁴ *Wallenberg Wood Science Center, Department of Fiber and Polymer Technology, KTH Royal Institute of Technology, 100 44 Stockholm, Sweden.*

⁵ *RISE Research Institutes of Sweden, Bio- and Organic Electronics, Bredgatan 35, 60221 Norrköping, Sweden.*

**Corresponding authors: Magnus Berggren (magnus.berggren@liu.se), and Isak Engquist (isak.engquist@liu.se).*

Characterizations

Morphology and Chemical composition

SEM: The structure of the modified WVs was analyzed by field emission scanning electron microscopy (FE-SEM, Hitachi S-4800, Japan) working at a low acceleration voltage of 1 kV, both before and after PEDOT:PSS infiltration. The samples were sputtered with a platinum/palladium conductive layer using a sputter coater (Cressington 208HR, UK). The samples were dried in different conditions (supercritical drying using liquid CO₂ or air drying, with and without solvent exchange to EtOH) after being carefully microtomed to obtain a smooth surface

Conductometric titration: The amount of total acidic groups in the modified WV was determined by conductometric titration with a Metrohm 856 Conductimeter according to SCAN-CM 65:02 after fine milling of the wood veneers. The samples were measured in duplicates.

UV-vis spectra of the spent reaction solutions were collected in the range 240-400 nm with a Shimadzu UV2550 spectrophotometer.

Lignin and monosaccharides content: Lignin content (Klason lignin) was determined by acid hydrolysis with 72% sulfuric acid at 121 °C according to TAPPI method TAPPI T222 om-02^[1]. The measures were repeated three times. Analysis of the neutral sugars was performed on a Dionex ICS-3000 high-performance ion-exchange chromatograph (Thermo Fisher Scientific Inc., USA) after acid hydrolysis. The samples were analyzed in duplicates and anhydrous factors were used for the monosaccharides (0,88 for xylose and arabinose, 0,90 for glucose, mannose, and galactose). The weight percentage of cellulose and hemicellulose were calculated using Meier's correlations, i.e. to calculate cellulose content, glucose from glucomannan was subtracted out from total glucose content using a 1:3.5 ratio of glucose: mannose.^[2]

Mechanical properties: The samples were cut in strips of 30 × 5 mm² (Longitudinal × Tangential). The samples were preconditioned for 48 h in a room at a controlled temperature of 22 °C and 50% relative humidity. The three-point bending tests were performed using an Instron 5944 (USA) equipped with a 500 N load cell. The tests were carried out with a support gap of 20 mm and a crosshead speed of 0.1 mm s⁻¹. A preload of 0.5 N and 10 mm min⁻¹ extension rate was applied (no data was captured during preload).

Electrical and Electrochemical measurements

Electrical conductivity

CWVs were cut in the size of 2.5 cm x 1 cm (length x width), while a 4 electrodes system was prepared by depositing layer by layer of chromium/gold (5 nm/95 nm of thickness, respectively) on a plastic substrate using an Ike evaporator. To improve the electrical contact between the rough surface of CWVs and the electrodes, a thin layer of carbon paste was carefully glued on top of each electrode before positioning the CWVs. A slight press was also applied before drying the testing cell at 50°C for 15 minutes. After that, the obtained cell (see Figure SI1) was measured using a 4-probe technique to study the sheet resistance and conductivity of CWVs. The Keithley 2400 source meter was used to supply the current to the two outer electrodes, and measured the voltage between the two inner electrodes using a 4-wires sensing mode.

Based on the obtained resistance, the electrical conductivity (σ) of CWVs is calculated using the below equation [3]:

$$\sigma = \frac{1}{\rho} = \frac{L}{RA} \quad (1)$$

with R is the obtained resistance, L is the distance between the two inner electrodes and A is the crosssectional area of the specimen (CWVs).

The sheet resistance of CWVs was calculated using the following equation:

$$R_s = \frac{1}{\sigma t} \quad (2)$$

, where R_s is the sheet resistance, t is the thickness of the sample.

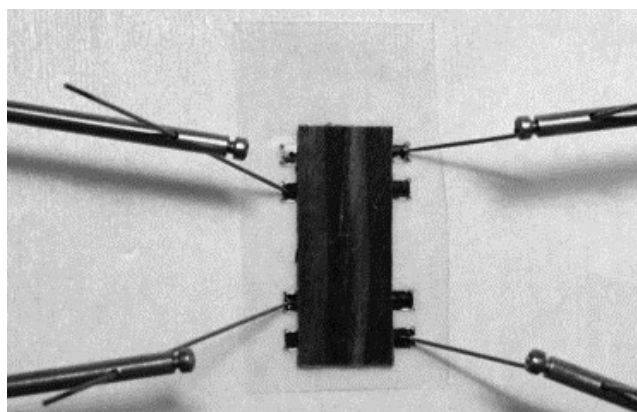


Figure SI.1. The testing cell in the electrical conductivity measurement.

Electrochemical measurements

CWV electrodes' preparation

The CWV-based supercapacitor electrodes were prepared as described in the below scheme:

The 2 centimeters long carbon fibers were attached to both the front and back sides of CWVs, which were cut in the size of 2.5 cm x 1 cm (length x width), using carbon paste as the glue material. After that, the electrodes were dried at 50°C for 15 minutes before drop-casting melted paraffin wax into the pack of carbon fibers (Figure SI2, Supporting Information). The paraffin-casted area was covered with a sticky tap, and the prepared electrode was kept at room temperature for 30 minutes before testing.

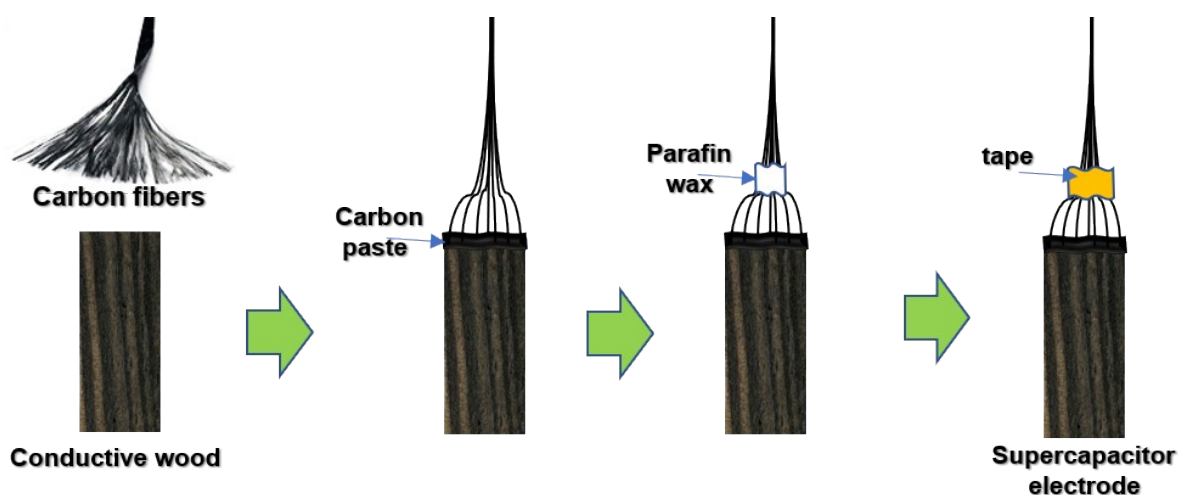


Figure SI.2. The preparation process of CWV-based supercapacitor electrodes.

Carbon-Felt/PEDOT:PSS (C-PP) electrode preparation

A carbon felt sheet was prepared in a size of 2.5 (cm) x 1 (cm) before being activated in a UV ozone oven for 30 minutes. The sheet, after that, was gradually drop-casted with 5 ml of the PEDOT: PSS: DMSO suspension and dried to obtain the C-PP template. The template was later used to prepare a C-PP supercapacitor electrode using the same method of preparing the CWV electrode.

Delignified-Wood/PEDOT:PSS (DWV-PP) electrode preparation

Delignified WVs (DWVs) were prepared by immersing the WVs in a NaClO₂ (3%) solution for 15 hours until the WVs turn into a clear and white sheet as shown in Figure SI3. The DWVs were, afterward, cleaned with DI water before impregnated into the PEDOT:PSS: DMSO

suspension and air-dried at 75°C to obtain the DWV-PP conductive wood. The DWV-PP conductive wood was later used to prepare the DWV-PP supercapacitor electrode in the same method as in preparing the CWV electrodes.

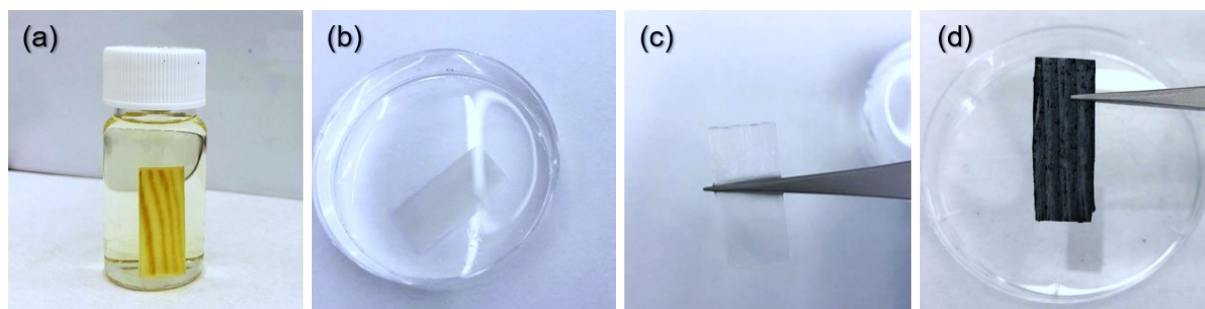


Figure. SI.3. a) WV delignificated in NaClO (3%), b) and c) Delignificated WVs (DWVs); d) PEDOT:PSS infiltrated DWVs (DWV-PP)

Electrochemical measurements and calculations

The electrochemical measurements were performed with a potentiostat/galvanostat (by Biologic, SP-200) coupled to a computer. The supercapacitor electrodes were measured in a three-electrode configuration system, while its devices were characterized using a two-electrode system. All parameters are the same in both systems.

The areal and specific capacitances of a single supercapacitor electrode are calculated from its GCD profiles by the following equations:

$$C_{(\text{area})} = \frac{I \times \Delta t}{S \times \Delta V} \quad (3)$$

$$C_{(\text{specific})} = \frac{I \times \Delta t}{m \times \Delta V} \quad (4)$$

where I is the discharge current, Δt is the discharge time, S is the effective area of the electrode, ΔV is the potential window of the discharge process, and m is the mass of the electrode.

The areal and specific capacitances of the supercapacitor devices are calculated from their GCD profiles according to the following equations:

$$C_{(\text{area})} = \frac{I \times \Delta t}{S \times \Delta V} \quad (5)$$

$$C_{(\text{mass})} = \frac{I \times \Delta t}{m \times \Delta V} \quad (6)$$

where I is the discharge current, Δt is the discharge time, S is the area of the electrode, ΔV is the voltage difference from the beginning to the end of an individual discharge cycle, and m is the total mass of the negative and positive electrode materials. In the calculation of areal-specific capacitance, the error bar represents the areal capacitance variation among different samples at a sulfonation time. However, the error bar in the mass-specific capacitance plot is representative of the capacitance variation caused by the mass measurement errors of PEDOT and lignin in one sample at a sulfonation time.

The supercapacitor devices' energy (E) and power densities (P) are calculated using the following equations:

$$E = \frac{C \times \Delta V^2}{2} \quad (7)$$

$$P = \frac{E}{\Delta t} \quad (8)$$

where C is the areal or specific capacitance of the ASC device, Δt and ΔV are the discharge time and potential difference of an individual discharge cycle

Results & discussion

Chemical composition of WV and SWVs

Table SI.1: Chemical composition (polysaccharides and lignin) by weight of the WV and SWV samples.

	Cellulose (wt.%)	Glucomannan (wt.%)	Xylan (wt.%)	Lignin (wt.%)
WV-native	41.8 ± 0.5	16.0 ± 0.4	5.7 ± 0.1	28.1 ± 0.5
SWV-1/2h	47.6 ± 0.1	16.3 ± 0.2	5.4 ± 0.1	22.1 ± 2.6
SWV-1h	51.8 ± 0.3	13.5 ± 0.1	5.4 ± 0.1	17.1 ± 1.2
SWV-3h	53.9 ± 0.6	13.7 ± 0.2	5.6 ± 0.1	16.5 ± 0.8
SWV-5h	55.4 ± 0.1	13.9 ± 0.1	5.1 ± 0.1	15.7 ± 1.0

The uronic acids are known to be degraded by acid hydrolysis with concentrated sulfuric acid, thus we did not quantify them for our samples. They can account for up to 5-6% of o.d weight for Scots pine [4].

Lignin removal and the total yield of the sulfonation process.

Table SI.2: Lignin removal (%) and the total yield of the sulfonation process.

	Lignin removed (%)	Total Yield (% on o.d. wood)	Sulfonation Degree (Strong acid content, $\mu\text{mol/g}$)
WV-native	0	100.0	9.0
SWV-1/2h	21.0	81.2	300.0
SWV-1h	39.1	80.2	315.0
SWV-3h	41.3	78.6	359.0
SWV-5h	44.1	63.5	375.0

Lignin concentration in spent reaction solutions

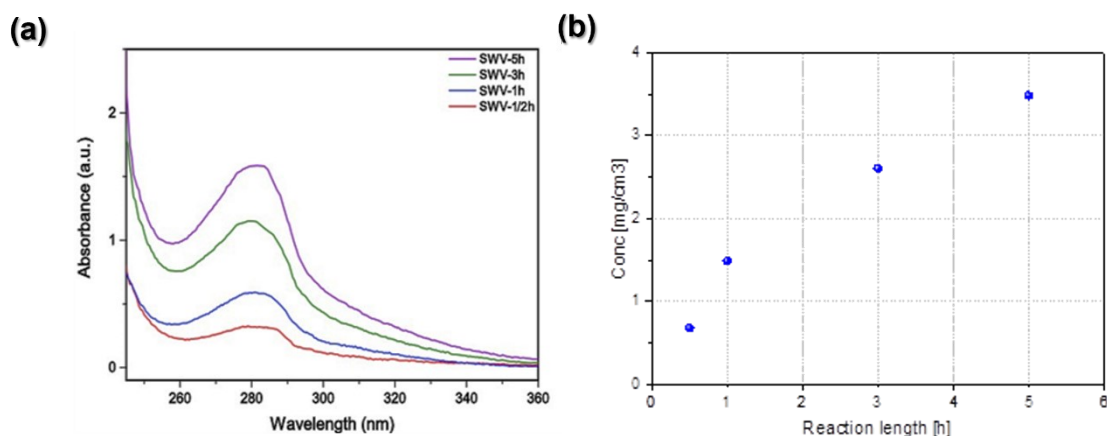


Figure SI.4: a) UV-Vis absorbance spectra of the post-reaction solutions from the SWV samples. The absorption peak at 280nm is associated with sulfonated lignin b) Lignin concentration in spent reaction solutions measured by UV-vis absorbance at 280 nm after background correction. The absorptivity value (ϵ) was chosen according to ^[5] and set to 11.9 ($l\ g^{-1}\ cm^{-1}$).

The samples' masses and PEDOT:PSS content

All samples including native-WV, SWVs, and CWVs were dried before measuring their weights. The mass density of WVs, SWVs, and CWVs and their PEDOT:PSS content were measured and presented in table SI.2 below.

Table SI.3: Samples' mass control

Samples	Native and SWVs (mg/cm ²)	CWVs (mg/cm ²)	PEDOT:PSS content in CWVs (mg/cm ²)	PEDOT:PSS fractions in CWVs (wt.%)	Thickness of CWVs (μ m)	Total mass of active materials in CWV electrodes (mg/2.5cm ²)
Native	35.1 \pm 0.1	37.7 \pm 0.1	2.6 \pm 0.2	7.0 \pm 0.5	720 \pm 10	\approx 31.2
½ h	28.5 \pm 0.1	31.7 \pm 0.1	3.2 \pm 0.2	10.0 \pm 0.8	710 \pm 10	\approx 23.8
1 h	28.1 \pm 0.2	32.1 \pm 0.2	4.0 \pm 0.4	12.5 \pm 1.3	690 \pm 10	\approx 22.1

3 h	26.8 ± 0.2	30.9 ± 0.2	4.1 ± 0.4	13.3 ± 1.4	670 ± 10	≈21.4
5 h	21.7 ± 0.2	26.1 ± 0.3	4.4 ± 0.5	16.9 ± 2.1	580 ± 30	≈19.6

PEDOT:PSS layer thickness

To acquire an estimation of the polymer thickness layer on the cell wall, an image analysis method was used to calculate the approximated inner surface of the cell lumen for our representative CWV-1h. The volume of the infiltrated PEDOT:PSS was obtained by dividing the loaded mass of polymer (~0,012g for CWV-1h) by its density found in literature (1,01 g/cm³ according to Sigma Aldrich).

The method employed one of the CWV-1h cross sections images, 500x500 μm² of size. The original SEM image was converted to a binary one (Figure SI 5a) and the areas of the circles (Figure SI 5b) were calculated and averaged by the software. The threshold of the areas was set between 20 and 1800 μm² to avoid speckles or big cracks to be included in the calculations. From the diameters of these circles, the areas of the approximated “cylinders”, were then obtained assuming uninterrupted lumens throughout the length of the sample (3 cm). The polymer thickness value obtained was ~700 nm.

The method is quite likely overestimating the thickness if we consider an expected bulkier polymer deposition on the outer surface of the veneer which has not been completely peeled off after infiltration.

To support these calculations, further imaging of the PEDOT:PSS layer, peeled off from the lumen after supercritical drying, was carried out. The peeled polymer layer in a representative lumen is presented in figure SI 7. Considering that the liquid CO₂ treatment is likely to have increased the width of the film as it is used to obtain aerogels from the polymer, the imaged polymer layer, showing thicknesses roughly between 200 and 600 nm, is in accordance with our calculations.

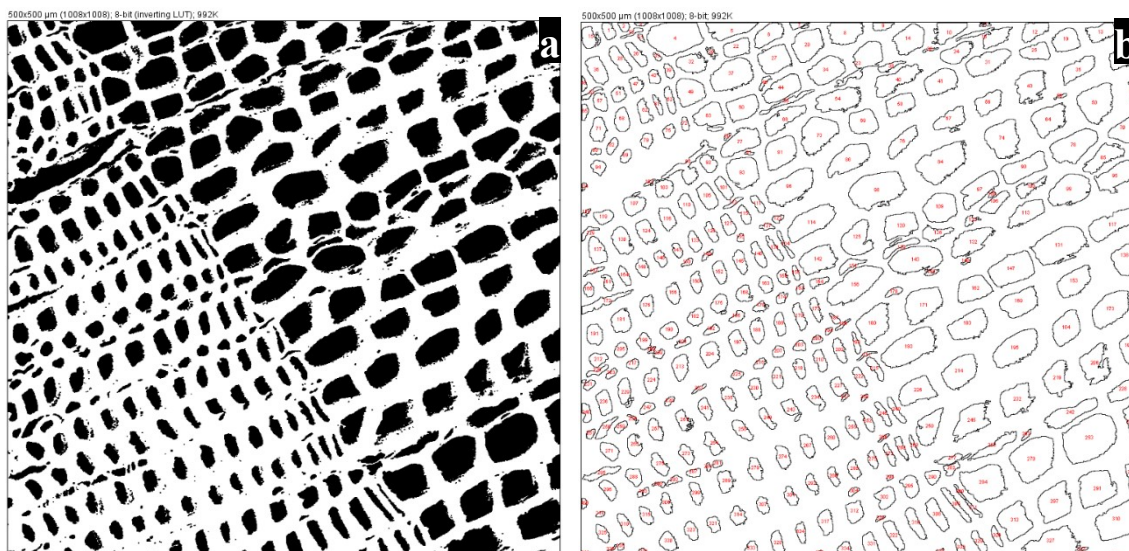
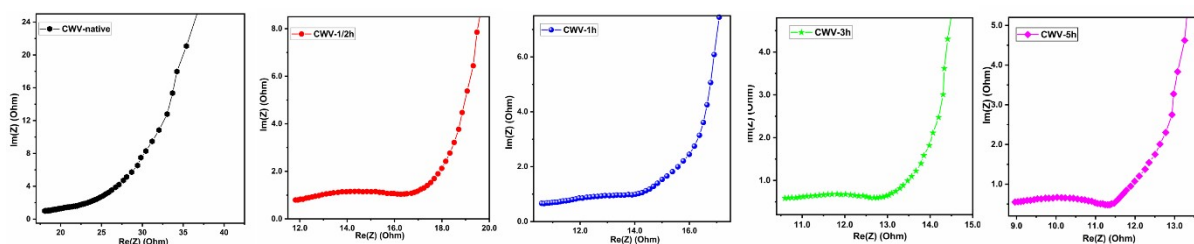


Fig. SI. 5: a) the binary image used for calculations, obtained from an SEM micrograph of CWV-1h, b) the same image, with every cell lumen outlined and counted. Image size: 500x500 μm².

The electrochemical impedance spectroscopy of CWVs

Table SI.4: Nyquist plots, Equivalent Series Resistance (ESR), and charge transfer resistance (R_{ct}) of WVCs.

	CWV-native	CWV-½ h	CWV-1 h	CWV-3 h	CWV-5 h
ESR (Ω)	18.1	12.8	10.6	10.5	9.0
R_{ct} (Ω)	NA	~4.5	~3.2	~2.3	~2.2



Electrolyte and microstructure of CWV electrode before and after cycling

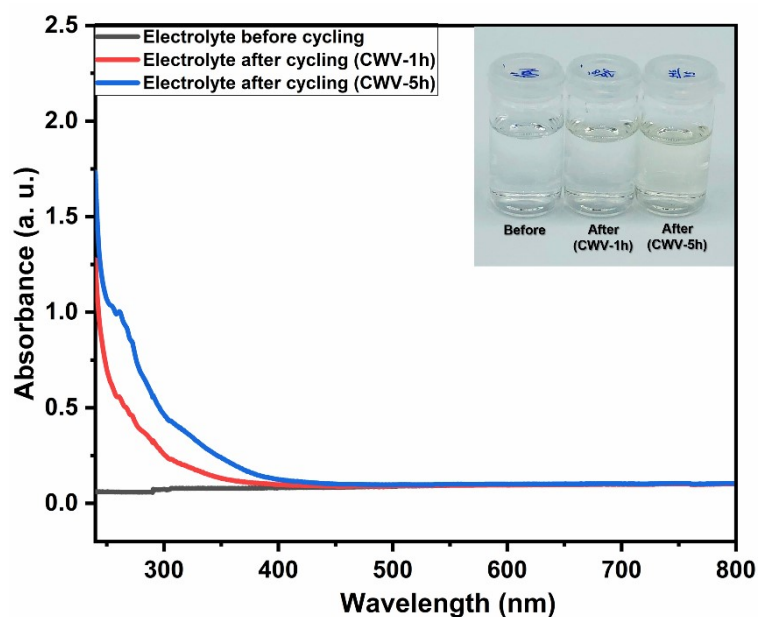


Fig. SI. 6. The UVvis spectra of the electrolyte (NaCl 1M) before cycling, and after cycling CWV-1h electrode or CWV-5h electrode.

In Figure SI.6, the UVvis spectra of the electrolyte after cycling have absorbance peaks below 400 nm, while there is no similar peak observed for the electrolyte before cycling. This suggests that there are chemical substances that leaked out from the CWV electrodes while cycling. Comparing the obtained results with our previous work [6], we presume that the chemical substance is probably lignosulfonate, and its dissolution could lead to the reduction of the electrode's capacitances.

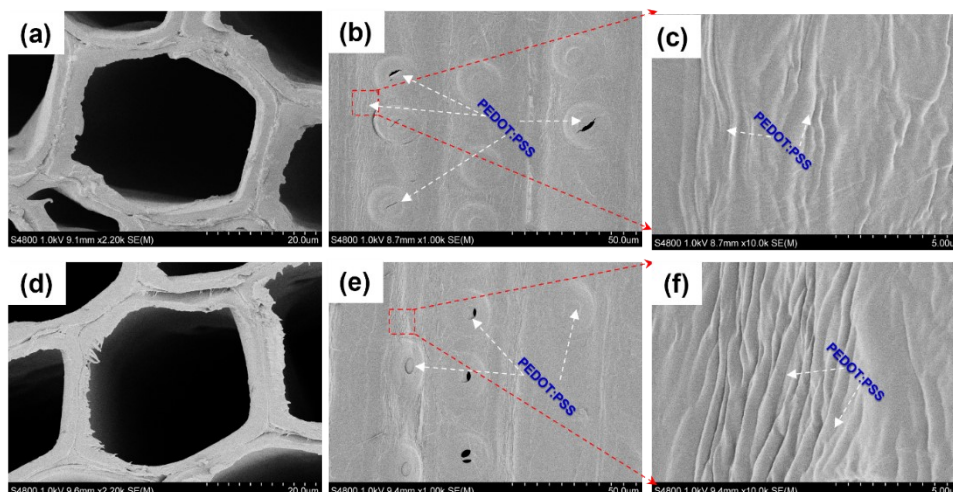


Fig. SI.7. The microstructure of CWV-1h electrode before and after cycling: The cross-sectional (a) and the longitudinal ((b) and (c)) SEM images of CWV-1h before cycling; The cross-sectional (d) and the longitudinal ((e) and (f)) SEM images of CWV-1h after cycling.

There are no major differences in the morphology of the wood and polymer before and after cycling.

Wood-based electrolyte

The reaction solution (RS-1h) obtained from the SWV-1h preparation process was used as a supercapacitor electrolyte to investigate the electrochemical properties of CWV-1h. The measurement setup is the same as in the measurement of CWV-1h in NaCl (1M) electrolyte.

In Figure SI.6a, the CV curve of CWV-1h in RS-1h electrolyte shows a different shape and the potential range in comparison with the curve of CWV-1h measured in NaCl 1M. The differences could be attributed to the different chemical compositions between the RS-1h and NaCl electrolyte. As we know, RS-1h probably contains diluted sulfonated lignin, hemicellulose, sodium sulfite, and wood extractives, thus the electrolyte should not present the same electrochemical properties as observed in NaCl. Although operated in a larger potential, RS-1h has a smaller CV curve area than that of NaCl. This indicates that CWV-1h will have a smaller charge storage capacitance in the RS-1h. The capacitance drop is mainly attributed to the chemical composition of the electrolyte, but also the reduction of PEDOT when the voltage sweep goes below -0.6 V. This recommends that it's unnecessary to study the charge storage capacity of the PEDOT: PSS-based electrode at the potential being below the reduction voltage, for example, below -0.6V in this work.

The CV curves at different scan rates of CWV-1h in RS-1h are shown in Figure SI6.b. At a higher scan rate, the curve remains a similar shape, but reaches a higher current, suggesting the good rate capability of the CWV-1h electrode. The capacitance of CWV-1h is evaluated based on GCD curves presented in figure SI6c, where the capacitance is normalized following either the area or the mass of the CWV-1h. At the current densities of 1.2, 1.6, 2.0, and 2.4 mA cm⁻², CWV-1h has the capacitance of 14.0, 12.1, 10.8, and 9.4 mF cm⁻², respectively. In comparison to the obtained capacitance in NaCl (1M), these values are about 55% smaller. The reduction is also related to the higher ESR (17.3 Ω vs. 10.6 Ω in NaCl) and R_{ct} (16.0 Ω vs. 3.2 in NaCl) numbers evaluated from the Nyquist plot in Figure SI6e.

Although the capacitance observed a strong reduction, the electrolyte shows good capacitance retention of 88.2% after 400 cycles and 77.3% after 1000 cycles. These numbers significantly surpass the 55.5% capacitance retention of CWV-1h in the NaCl (1M) electrolyte. We see this as an indication that rest products like the RS could prove to be useful and economic alternatives to other electrolytes

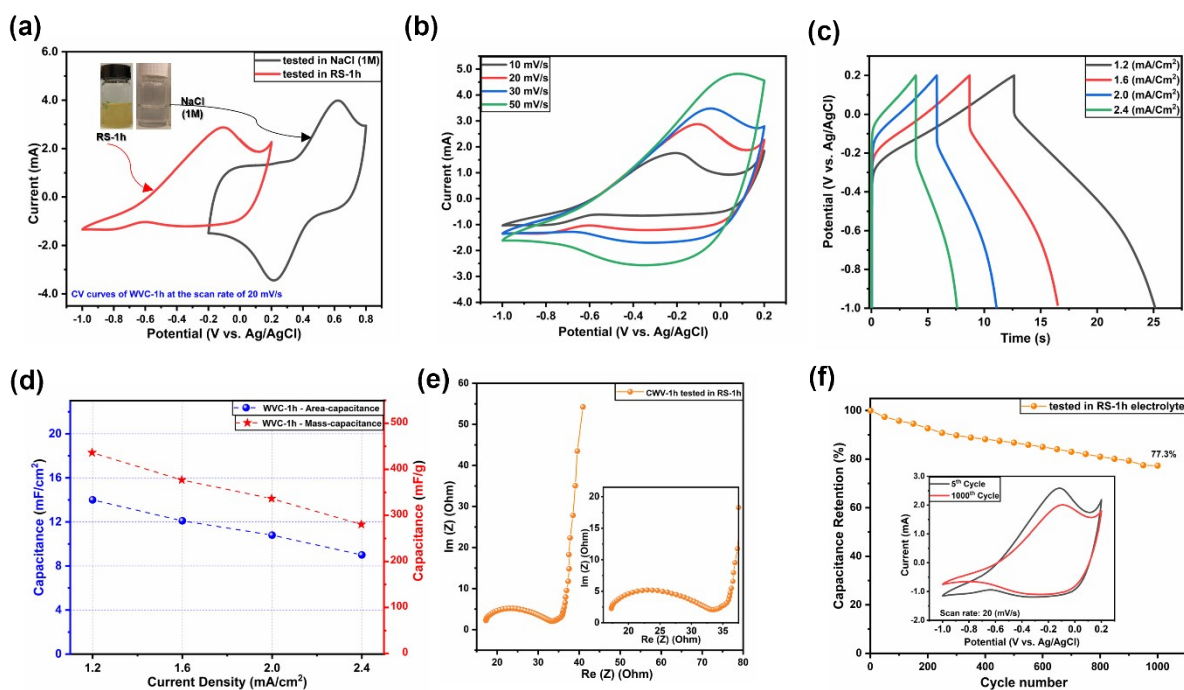


Fig. SI.8: a) CV curves of CWV-1h in RS-1h and NaCl(1M) electrolytes at the same scan rate of 20 (mV/s); b) CV curves of CWV-1h in RS-1h electrolyte at different scan rates; c) GCD curves of CWV-1h in RS-1h electrolyte at different current densities; d) Area- and Mass- Capacitance of CWV-1h at different current densities; e) Nyquist plot of CWV-1h in RS-1h electrolyte at the frequency range of 50 mHz to 100 kHz (inset: the Nyquist plot of CWV-1h at the high frequency); Cyclic stability of WVC-1h in RS-1h electrolyte (inset: The CV curves of CWV-1h at the 1st and 1000th cycles).

Mechanical measurements

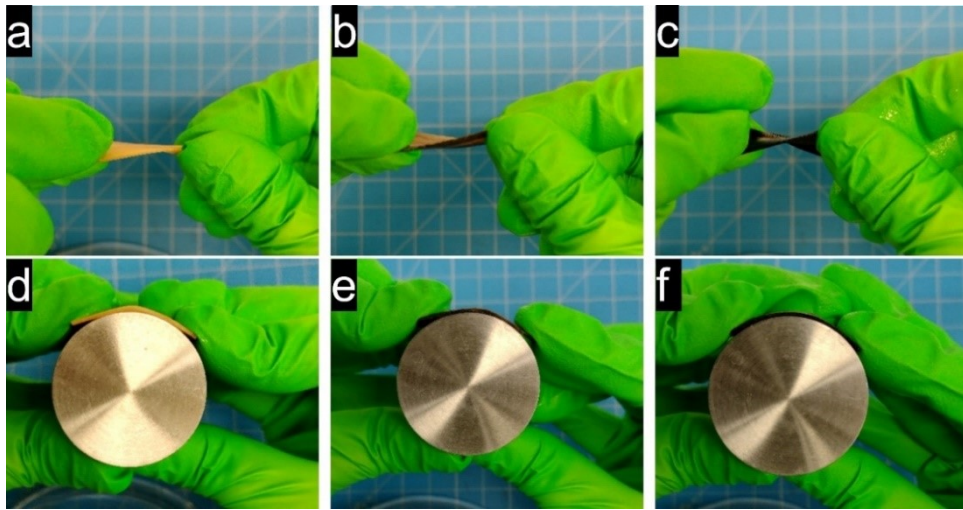


Fig. SI. 9: Photos showing the flexibility of WV, and CWVs samples in wet conditions. a) Twisting and d) bending of WV samples; b) Twisting and e) bending of CWV-Native samples; c) Twisting and f) bending of CWV-1h samples.

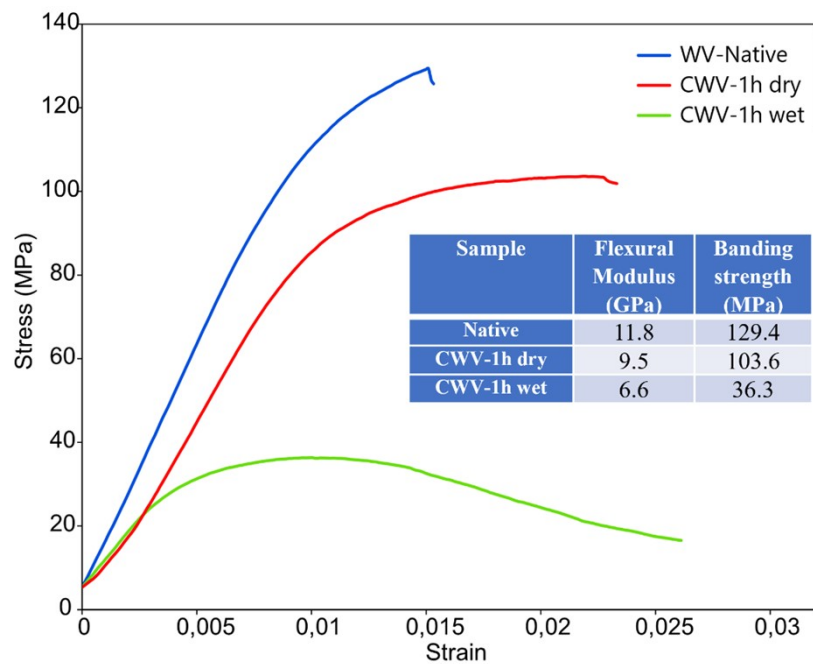


Fig. SI.10: Results of 3-point bending tests on WV-Native (dry) and CWV-1h (wet and dry state) samples.

The results in Figure SI.10 suggest that CWV-1h in dry state is mechanically resistant with flexural modulus and bending strength that are comparable to those of native wood sample (WV-Native). On the contrary, in wet state, the CWVs show a high degree of flexibility (Fig. SI.9c and SI.9f) compared with WV-Native and its respective CWV-Native (SI.9a, b, d,e).

Wood Supercapacitor (WS)

A wood supercapacitor was fabricated by using CWV-1h (2.5 x1 cm²) and DWV-PP (2.5 x1 cm²) as its electrodes, while a 140 μm thick of SWV-1h was used as the device separator (as shown in the inset of Figure SI.7a). NaCl 1M was used as the supercapacitor electrolyte so that a fair comparison could be made for the electrochemical properties between the device and its single electrodes. In Figure SI.7a, the CV curves of CWV-1h and DWV-PP present distinct properties. While the earlier exhibits the property of an asymmetric supercapacitor electrode, the latter represents the characteristic of an EDLC electrode with a near rectangle CV curve. Accordingly, the CV curves of the full device shown in Figure SI.7b are the combination of the two single electrodes' characteristics. All CV curves have a pair of faradaic redox-reaction peaks, which correspond to the pseudocapacitive properties of sulfonate lignin in the CWV-1h electrode. Besides that, at a higher scan rate CV curve reach a higher current, suggesting the good reversible redox reaction and rate capability of the device. GCD curves of the device are given in Figure SI7.c showing corresponded properties to its CV curves. At a lower current density, the discharge time of the device is longer. The area-specific capacitance of the device is evaluated using the data Figure SI.7c and the area of the single electrode. At the current densities of 1.2; 1.6; 2.0; 2.4 mA cm⁻², the device has a capacitance of 19.0; 17.9; 16.6; 15.6 mF cm⁻², respectively.

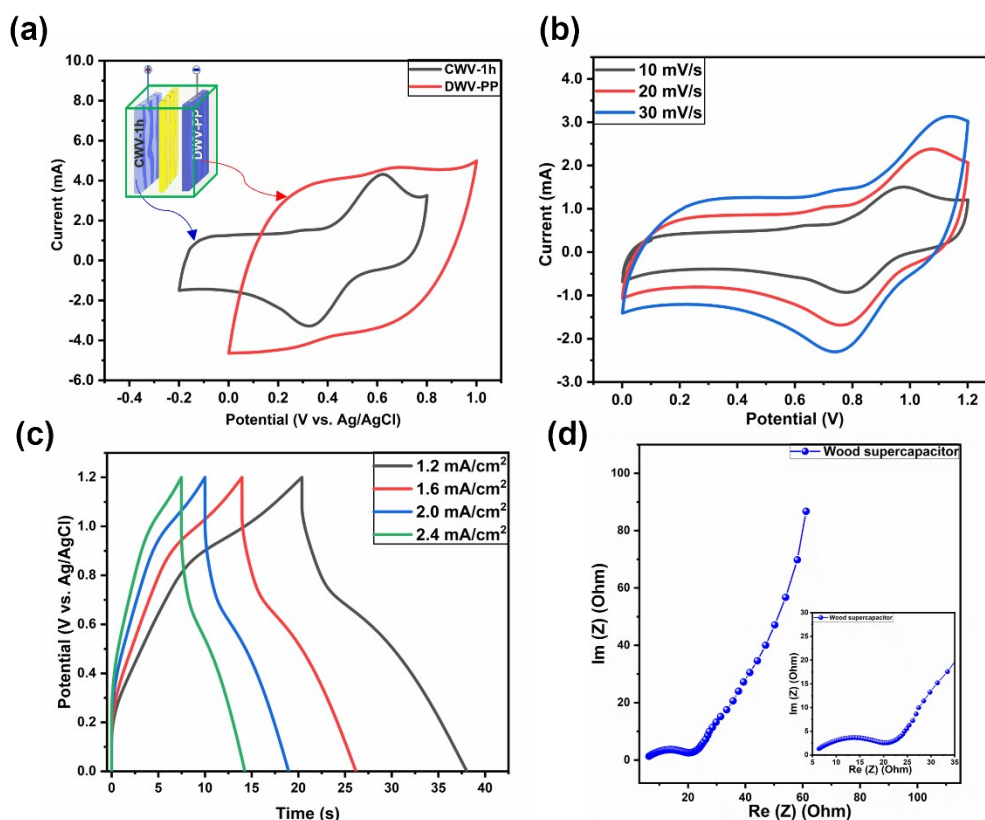


Fig. SI. 11: a) The CV curves of WVC-1h and DW-PP at the same scan rate of 20 (mV/s) (Inset: A brief illustration of the WS); b) CV curves of the WS at different scan rates; c) The charge/discharge (GCD) curves of the wood supercapacitor at different current densities; e) Nyquist Plot of the wood supercapacitor at the frequency range of 50 mHz to 100 kHz (inset: the Nyquist plot at the high frequency)

In Figure SI.7d, the Nyquist plot of WS consists of a near semicircle at the high frequency and a straight curve at the low frequency, indicating the potential charge transport property of a supercapacitor. The ESR of WS is 6.4 Ω , while its charge transfer resistance (R_{ct}) is 13.5 Ω .

The thick PEDOT:PSS coating layer is partly removed from the CWV surface.



Figure SI 12: The thick coating layer of PEDOT:PSS is removed partly from the CWV-5h surface.

Table SI.5. Recent progress in wood -based supecapacitor electrodes and devices.

<i>Active materials/wood</i>	<i>Electrode's Specific capacitance</i>	<i>Device's specific capacitance</i>	<i>Active materials' morphology</i>	<i>Capacitance contribution from native lignin</i>	<i>Ref.</i>
Native lignin/PEDOT:PSS/wood	4.9 F/g 38 mF/cm ²	22.9 mF/cm ²	Nano thinfilm	Yes	This work
PANI/CNT/ wood	186.58 F/g	0.71 F cm ²	Nanoparticles on nanotubes	No	7
PANI/RGO/wood	931.92 F/g	0.78 F/cm ²	Nanoparticles on 2D microsheat	No	8
PANI/Wood	218.75 F/g	0.12 F cm ²	Nanoparticles	No	9
PANI- PPy/wood	360 F/g	---	Nanoparticles	No	10
PANI/Wood	800 F/g	---	Nano-, micro-fibers	No	11
PPy/RGO/wood	848.01 F/g	0.89 F/cm ²	Nanoparticles on 2D microsheat	No	8
PPy/Wood	1710 mF/cm ²	1210 mF/cm ²	Nanoparticles	No	12
PPy/lignosulfonate powder/wood	---	1062 mF/cm ²	Gel-like	No	13
PANI/CNT/carbonized wood	1019.5 F/g	25.1 F/cm ³	Core-shell nanotube	No	14
PANI/carbonized wood	639.5 F/g	---	Micro-particles	No	15
S-/N-doped carbonized wood	704 F/g	135 F/g	Wood carbon	No	16
MoSe ₂ /carbonized wood	1043 mF/cm ²	---	Nano flower in wood carbon	No	17
Polylamine/CuO ₂ / milled wood carbon.	694.8 F/g	50.1 F/g	Microparticles and flakes in wood carbon	No	18
MnO ₂ /carbonized wood	4155 mF/cm ²	3600 mF/cm ²	Nanoparticles in wood carbon	No	19

Notes: PANI is polyaniline, PPy is polypyrrole, CNT is carbonanotube, and RGO is reduced graphene oxide.

References:

1. T. Tappi, 2002–2003 TAPPI Test Methods, **2002**.
2. H. Meier, *Acta Chem. Scandinavia*, 1958, **12**, 1911-1918.
3. Y. Singh, *International Journal of Modern Physics: Conference Series*, 2013, **22**, 745-756.
4. R. C. Pettersen, in *The Chemistry of Solid Wood*, American Chemical Society, 1984, **207**, 57-126.
5. S.Y., Lin, and C. W. Dence (eds). *Methods in Lignin Chemistry*. Springer Series in Wood Science, Springer, Berlin, Heidelberg **1992**.
6. J. Edberg, O. Inganäs, I. Engquist, M. Berggren, *J. Mater. Chem. A*, 2018, **6**, 145-152.
7. S. Ke, D. Xie, K. Zhang , F. Cheng, and Y. Wu, *Mater. Adv.*, 2022, **3**, 2026-2036.
8. S. Lyu, Y. Chena, S. Han, L. Guo, N. Yang, and S.Wang, *RSC Adv.*, 2017, **7**, 54806-54812.
9. S. Ke, T. Ouyang, K. Zhang, Y. Nong, Y. Mo, Q. Mo, Y. Wei, and F. Cheng., *Macromol. Mater. Eng.*, 2019, **304**, 1900112-1900121.
10. J. Li, and Y. Jiao, *Front. Agr. Sci. Eng.*, 2019, **6**, 137-143.
11. C. Xiong, M. Li, S. Nie, W. Dang, W. Zhao, L. Dai, Y. N, *J. Power Sources*, 2020, **471**, 228448-228457.
12. G. G. Mastantuoni, V. C. Tran, I. Engquist, L. A. Berglund, Q. Zhou, *SSRN*, 2022, <https://dx.doi.org/10.2139/ssrn.4074343>.
13. Zhicheng Zhang, Chuying Yu, Zhiyuan Peng & Wenbin Zhong, *Cellulose*, 2021, **28**, 389–404.
14. W. Wu , X. Wang, Y. Deng, C. Zhou, Z. Wang, M. Zhang, X. Li, Y. Wu, Y. Luo, and D. Chen, *Nanoscale*, 2020, **12**, 17738-17745.
15. M. Cui, F. Wang, Z. Zhang, S. Min, *Electrochim. Acta*, 2020, **359**, 136961-136967
16. Z. Tang, Z. Pei, Z. Wang, H. Li, J. Zeng, Z. Ruan, Y. Huang, M. Zhua, Q. Xue, J. Yu, C. Zhi, *Carbon*, 2018, **130**, 532-543.
17. S. Wei, C. Wan, Y. Jiao, X. Li, J. Li, and Y. Wu, *Chem. Commun.*, 2020, **56**, 340-343.

18. C. Wan, W. Tian, J. Zhou, Y. Qing, Q. Huang, X. Li, S. Wei, L. Zhang, X. Liu, Y. Wu, *Mater. Des.* 2021, **198**, 109309-109320.

19. C. Chen, Y. Zhang, Y. Li, J. Dai, J. Song, Y. Yao, Y. Gong, I. Kierzewski, J. Xie, and L. Hu, *Energy Environ. Sci.*, 2017, **10**, 538-545.